American Mineralogist, Volume 78, pages 469–476, 1993

Micro-Raman and infrared spectral study of forsterite under high pressure

S. Y. Wang, S. K. Sharma, T. F. Cooney
Hawaii Institute of Geophysics, School of Ocean and Earth Science and Technology (SOEST), University of Hawaii at Manoa, 2525 Correa Road, Honolulu, Hawaii 96822, U.S.A.

Abstract

Raman and mid-IR spectra of synthetic forsterite (Mg_2SiO_4) have been recorded under pressure to about 200 kbar. Multichannel micro-Raman spectroscopy has made it possible to measure the forsterite spectra with high signal to noise ratio. Twenty-one bands are identified in the Raman spectrum of forsterite. Pressure dependencies of the frequencies of two of the Raman bands have been determined for the first time. All of the Raman bands move progressively to higher frequencies with increasing pressure. The frequency shift displays a linear relation with respect to pressure up to 70 kbar. The Raman peak at 585 cm^{-1}, usually attributed to a single vibrational mode, is in fact a doublet. The pressure derivatives of the bands in 585-cm^{-1} doublet are slightly different but do not change abruptly in the pressure range studied in our work. We also found that two Raman modes (424 and 441 cm^{-1}) are still present in our spectra in the pressure range of 100–200 kbar, in contrast to previously reported results. There is a slight break in the slopes of the five Raman bands in the pressure range 70–90 kbar. These changes in the slope are attributed to a change in the compression mechanism of forsterite at high pressures. Frequencies of six infrared-active internal modes of forsterite change linearly with pressure to 184 kbar, in agreement with the results of previous workers. The pressure dependencies of the infrared bands reported by various workers, however, show much larger variations than those of corresponding Raman bands. Observed changes in the relative intensities of the infrared bands at high pressures are attributed to the deformation of the SiO_4 tetrahedra above 81 kbar.

Introduction

Forsterite (Mg_2SiO_4) is a major constituent of the upper mantle (Akimoto et al., 1976). Cr-activated forsterite single crystals were recently found to be excellent materials for near-infrared lasers (Petricevic et al., 1988; Sugimoto et al., 1989). Raman and infrared spectra of forsterite have been measured extensively at ambient and high pressures to understand its lattice-dynamics and to determine the pressure dependence of heat capacity and entropy (Iishi, 1978; Xu et al., 1983; Besson et al., 1982; Hofmeister, 1987; Hofmeister et al., 1989; Lam et al., 1990; Chopelas, 1990; Gillet et al., 1991; Guyot and Reynard, 1992; Reynard, 1991). Chopelas (1990) has measured the pressure dependence of the Raman spectrum for forsterite to >200 kbar and suggested the possibility of a second-order phase transition above 91 kbar. The IR data in the middle IR range on forsterite were studied at pressures up to 300 kbar (Hofmeister et al., 1989; Xu et al., 1983). Far-IR spectra of forsterite were studied at pressures up to 425 kbar (Hofmeister et al., 1989). The band positions of forsterite and assignments at ambient pressure have been established (Hofmeister, 1987). Furthermore, mode Grüneisen parameters, γ_i; heat capacity, C_v; and entropy, S, have been calculated from $d\nu/dP$ using statistical thermodynamics of the lattice vibrations (Hofmeister et al., 1989; Chopelas, 1992; Gillet et al., 1991). Kudoh and Takéuchi (1985) investigated the structure of forsterite under high pressure up to 149 kbar and suggested change in the compression mechanism above 80 kbar. Evidently the structure of forsterite above 80 kbar is not well understood at present.

The present paper reports our results on the pressure dependence of 21 Raman bands of forsterite up to 204 kbar under hydrostatic pressure transmitting medium and up to 189 kbar with KBr as a quasi-hydrostatic pressure medium. For comparison with previous IR spectroscopy of forsterite at high pressure, we measured mid-IR data on forsterite under quasi-hydrostatic pressure up to 184 kbar.

Experimental methods

The forsterite used was a synthetic crystal from John B. Bates, Oak Ridge National Laboratory. Raman spectra were excited with the 457.9-nm line of an Ar ion laser; typical laser powers ranged from 60 to 80 mW. The laser light entered the diamond-anvil cell (DAC) at an angle of 35° from the normal to the diamond face. Raman spectra were obtained in 165° geometry using a Spex 1877 triple spectrometer (Sharma and Urmos, 1987; Sharma, 1990). Either an optical multichannel analyzer (OMA) or a

0003–004X/93/0506–0469$02.00

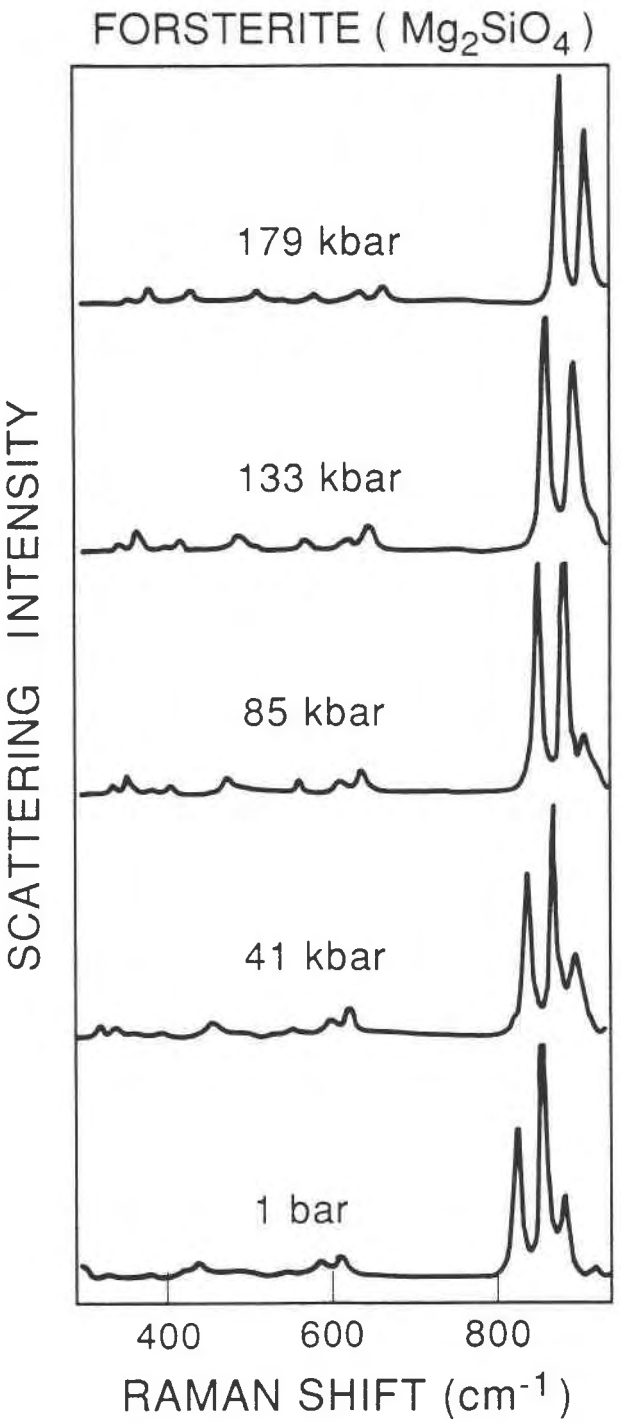

Fig. 1. Raman spectra of forsterite from 1 atm to 179 kbar and 18 °C under hydrostatic pressure conditions.

charge-coupled device (CCD) detection system was used for recording the data. The OMA detector temperature was set at −30 °C for minimizing dark noise. The CCD detector temperature was about −120 °C, with dark noise close to zero. These operating conditions made possible long exposures. The range of frequencies for the spectra of samples at pressure was 100–1100 cm^{-1}. All spectra were recorded at 291 ± 1 K.

Samples were randomly shaped (~0.03 mm) forsterite grains; micrometer-sized ruby grains were used for pressure calibration. In one set of experiments a 16:3:1 methanol to ethanol to H_2O liquid mixture was used as a pressure medium (Jayaraman, 1983). In the second set of experiments KBr was used as the pressure medium. In the case of the liquid mixture the pressure is hydrostatic, at least up to 100 kbar. This set of experiments is, therefore, referred to in the text as hydrostatic pressure experiments. The solid pressure-transmitting medium KBr provided a quasi-hydrostatic environment both at lower (<100 kbar) and higher pressure and is therefore referred to as a quasi-hydrostatic medium.

Pressures were generated with a megabar Mao-Bell type diamond-anvil cell (DAC) (Mao and Bell, 1978). The gasket was a 718 stainless steel plate, 0.15 mm thick and with a 0.15-mm hole. In both cases of hydrostatic and nonhydrostatic pressure, ruby fluorescences R_1 and R_2 were well resolved up to maximum pressure. In our experiments, the ruby fluorescence R_1 and R_2 bands did not broaden significantly until maximum pressure was reached. We also found that the pressure gradient in the cell did not change abruptly. The pressure differences in the cell, estimated from ruby fluorescence shift (Mao et al., 1978), did not exceed ±0.5 kbar under hydrostatic conditions and ±2.5 kbar under quasi-hydrostatic conditions.

IR spectra were analyzed using a Perkin-Elmer FT IR 1720× spectrometer. The range of frequencies for IR spectra was 400–4000 cm^{-1}, and the typical experimental conditions utilized a resolution of 4 cm^{-1}, a gain of 8×, and 1000–2000 scans. A pair of type IIa diamond anvils was used in the DAC. The range of frequencies analyzed in this work was 400–1400 cm^{-1}. The gasket material was a Mo plate 0.15 mm thick. To obtain data on weak peaks, the gasket, which had an aperture of 0.25–0.4 mm, was compressed to a thickness of 0.01–0.02 mm before loading the sample. Samples were loaded in the gasket in three configurations: (1) forsterite powder compressed to form a thin film on one anvil, a gasket placed between two anvils and filled with KBr in the gasket hole, and ruby chips placed on the top; (2) the gasket hole filled first with KBr powder, then filled with forsterite powder, ruby chips placed on the top of the sample; (3) the gasket hole filled with a mixture of 4:1 KBr to forsterite, then ruby chips placed on the top of the mixture (strictly speaking, the mixture ratio is determined by the depth of hole and the absorbance of sample). We obtained the same results from the three configurations.

The pressure was determined by ruby fluorescence from the ruby grains in DAC, which was excited by the 488.0-nm line of an Ar ion laser and was analyzed by a Spex 1403 double spectrometer through an optical fiber cable (Sharma et al., 1992). The values of pressure reported here are the average of pressures measured at three points in the DAC.

Table 1. Pressure derivatives, mode Grüneisen parameters, γ_i, and mode assignments for Raman vibrational modes of forsterite

No.	ν_{io} (cm^{-1})	$d\nu_i/dP$ (cm^{-1}/kbar) Hydrostatic	Nonhydrostatic	Chopelas* <91 kbar	Chopelas* >91 kbar	γ_{io}** Hydrostatic	Nonhydrostatic	Chopelas' data	Mode type†
1	183	0.301	0.301	0.303		2.150	2.150	2.090	T(MgII, SiO_4)
2	227	0.114	0.119	0.120	0.105	0.643	0.671	0.674	T(SiO_4, MgII)
3	244	0.235	0.226	0.230		1.232	1.186	1.210	T(SiO_4)
4	290	0.306	0.299			1.351	1.320		T(MgII)
5	306	0.326	0.368	0.390	0.305	1.364	1.539	1.630	T(MgII, SiO_4)
6	331	0.295	0.290	0.300		1.144	1.121	1.116	T(MgII)
7	341	0.473	0.444	0.498	0.402	1.775	1.667	1.870	R(SiO_4)
8	376	0.369	0.376	0.368		1.256	1.280	1.250	R(SiO_4)
9	411	0.312	0.330	0.318		0.972	1.028	0.990	R(SiO_4) + ν_2
10	424	0.480	0.421	0.475		1.449	1.271	1.430	R(SiO_4) + ν_2
11	434	0.458	0.471	0.474		1.351	1.389	1.400	R(SiO_4) + ν_2
12	441	0.545	0.518	0.550		1.585	1.503	1.600	R(SiO_4) + ν_2
13	545	0.179	0.196	0.225	0.131	0.420	0.460	0.528	ν_4
14	584	0.218	0.289	0.300	0.249	0.478	0.633	0.659	ν_4
15	587	0.280				0.611			ν_4
16	609	0.324	0.348	0.335		0.682	0.731	0.704	ν_4
17	826	0.307	0.344	0.312		0.476	0.533	0.483	(40% ν_1 + 60% ν_3)
18	856	0.285	0.257	0.327	0.267	0.426	0.384	0.489	(60% ν_1 + 40% ν_3)
19	884	0.303	0.354	0.303		0.439	0.512	0.439	ν_3
20	922	0.276	0.302	0.275		0.383	0.419	0.382	ν_3
21	966	0.501	0.504	0.499		0.663	0.668	0.661	ν_3

* Chopelas (1990).
** Calculated from $(K_{TO}/\nu_{io})(d\nu_i/dP)_{TO}$, where K_{TO} is 1280 kbar (Webb, 1985; Kumazawa and Anderson, 1969; Graham and Barsch, 1969).
† Iishi (1978); Hofmeister (1987); Lam et al. (1990); Chopelas (1991) where T = translational; R = rotational; ν_{1-4}, internal SiO_4; MgII, $Mg2O_6$ modes.

Results and discussion

Raman spectral data

Forsterite has an orthorhombic unit cell (space group *Pbnm*; $Z = 4$) and three types of polyhedra—$Mg1O_6$ octahedra, $Mg2O_6$ octahedra, and SiO_4 tetrahedra (e.g., Brown, 1980). On the basis of factor-group analysis, it has been shown that forsterite has 84 modes of vibrations. Out of these modes 36 are Raman active, 35 are infrared active, ten are inactive, and three are acoustic modes (e.g., Iishi, 1978; Hofmeister, 1987; Chopelas, 1990; Lam et al., 1990). The 36 Raman active modes of forsterite that are theoretically expected have been identified with polarized single-crystal Raman measurements (Iishi, 1978; Lam et al., 1990; Chopelas, 1991). Observation of fewer Raman bands at high pressure (Fig. 1, Table 1) is partly due to accidental degeneracies, weak intensities, or both. Random orientation of the forsterite grain and the restricted geometry of DAC make it difficult to detect and resolve weak bands. The ambient Raman frequencies of forsterite, their pressure dependencies, and assignments are summarized in Table 1.

Lam et al. (1990) have discussed the origin and mixed characters of the internal modes of SiO_4 in forsterite at ambient pressure. They found that interaction between tetrahedra produces perturbation of the eigenmodes of an isolated tetrahedron causing (1) lifting of degeneracies of the modes, (2) increase in mode frequencies because of an additional force constant, and (3) mixture of the different symmetries of the unperturbed modes (ν_3, ν_1, ν_4, ν_2). The calculations of Lam et al. (1990) have shown that (1) the difference in the ν_3 and ν_1 frequencies is proportional to the Si-O force constant; (2) the ν_4- and ν_2-derived modes are most sensitive to the increase in O-O force constants; (3) the intertetrahedral O-O force constants increase the frequency of the ν_1-derived mode more than those of the ν_3-derived mode, and (4) the Mg-O interaction increases the frequencies of the ν_4- and ν_2-derived modes more than those of ν_3- and ν_1-derived modes.

It is interesting to note that the pressure dependencies of the A_{1g} modes 826, 856, and 966 cm^{-1}, under hydrostatic conditions up to 85 kbar, are 0.307, 0.285, and 0.501 cm^{-1}/kbar, respectively (Table 1). These pressure dependencies are consistent with the respective percentages of ν_3 character of the corresponding modes (Table 1). The 966 cm^{-1} mode has 100% ν_3 character. Therefore, one expects that its frequency would show a significant increase with pressure because of the shortening of Si-O bonds.

Figure 2a and 2b show the pressure dependence for 21 Raman modes under hydrostatic pressure and 20 Raman modes under nonhydrostatic pressure, respectively.

The pressure derivatives, $d\nu/dP$, and mode Grüneisen parameters, γ_i, calculated from the equation

$$\gamma_i = (K_{TO}/\nu_{io})(d\nu_i/dP)_{TO} \quad (1)$$

(Chopelas, 1990) are listed in Table 1, where $K_{TO} = 1280$ kbar, the bulk modulus of forsterite at 1 atm, and room temperature (Graham and Barsch, 1969; Kumazawa and Anderson, 1969).

The pressure responses of various modes do not exhibit large differences between hydrostatic and quasi-hydrostatic pressure conditions (Table 1). The bands at 227,

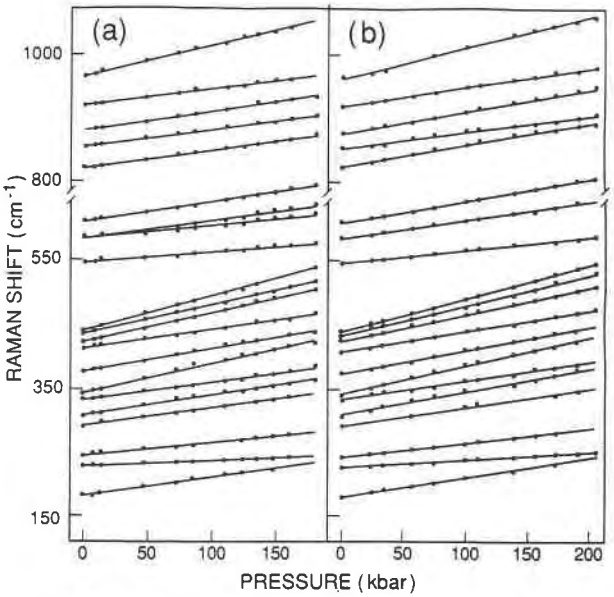

Fig. 2. The pressure dependence for Raman modes under (**a**) hydrostatic and (**b**) quasi-hydrostatic pressure.

306, 331, 341, 376, 434, 545, 584, 587, 609, 826, 884, 922, and 966 cm^{-1} have medium or strong intensities. The determination of their frequencies is comparatively reliable. At high pressure, the intensity of some peaks decreases markedly. Peaks 20 (922 cm^{-1}) and 21 (966 cm^{-1}) merge progressively into a strong C-O stretch band of alcohol (Mammone et al., 1980a) as pressure increases, so their positions are difficult to measure accurately when alcohol is used as a pressure-transmitting medium. Figure 2 shows that all of the Raman peaks move to progressively higher frequencies as pressure increases and that frequency shifts have a linear relation with pressure.

Besson et al. (1982) reported high-pressure Raman spectra of forsterite in the high-frequency region up to 65

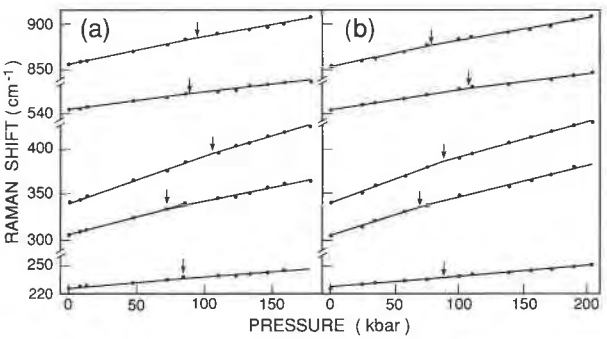

Fig. 3. The change of slope of pressure dependence for five Raman modes of forsterite under (**a**) hydrostatic pressure and (**b**) quasi-hydrostatic pressure. Arrows mark the points of break in the slope.

kbar and estimated pressure dependencies of the bands at 826, 856, and 922, respectively, as 0.35, 0.34, and 0.39 cm^{-1}/kbar. Our results show that the pressure dependencies of the bands at 826 and 856 cm^{-1} under quasi-hydrostatic pressure (Table 1) are close to the values reported by Besson et al. (1982); however, the pressure dependence of the 922-cm^{-1} band under quasi-hydrostatic pressure is 0.302 cm^{-1}/kbar, lower than that estimated by Besson et al. In general, our results on the pressure dependencies of the 19 Raman bands are in agreement with the results of Chopelas (1990) in the pressure range of 0.001–91 kbar. The pressure dependencies of two additional bands at 290 and 587 cm^{-1} that we were able to detect under hydrostatic pressures are, respectively, 0.306 and 0.280 cm^{-1}/kbar (Table 1).

Our $d\nu_i/dP$ and γ_i values are close to those measured by Chopelas, and we also found that above a certain pressure the slopes of some Raman modes vs. pressure seem to change slightly. These changes are not distinct. Under hydrostatic pressure, the Raman bands 227, 306, 341, 545, and 856 cm^{-1} show a break in their slope, respec-

Table 2. Standard deviation of linear fit for Raman shift pressure of forsterite

No.	Freq. ν_{i0}	Pressure derivatives $d\nu_i/dP$ (cm^{-1}/kbar)			Standard deviation	
		Whole range 0–179 kbar	Respective range 0–85 kbar	Respective range 109–179 kbar	Whole range fit	Respective range fit
			Hydrostatic pressure			
2	227	0.114	0.122	0.109	±0.001	±0.001
5	306	0.326	0.386	0.304	±0.006	±0.004
7	341	0.473	0.473	0.498	±0.008	±0.004
13	545	0.179	0.195	0.175	±0.004	±0.003
18	856	0.285	0.309	0.256	±0.003	±0.003
			Nonhydrostatic pressure			
2	227	0.119	0.120	0.112	±0.002	±0.002
5	306	0.368	0.433	0.353	±0.009	±0.006
7	341	0.444	0.505	0.382	±0.006	±0.003
13	545	0.196	0.200	0.166	±0.006	±0.002
18	856	0.257	0.311	0.237	±0.006	±0.005

Note: Standard deviation $= \left[\sum_{i=1}^{n} (\nu_i - \bar{\nu}_i)^2\right]^{1/2} \Big/ (n-2)$.

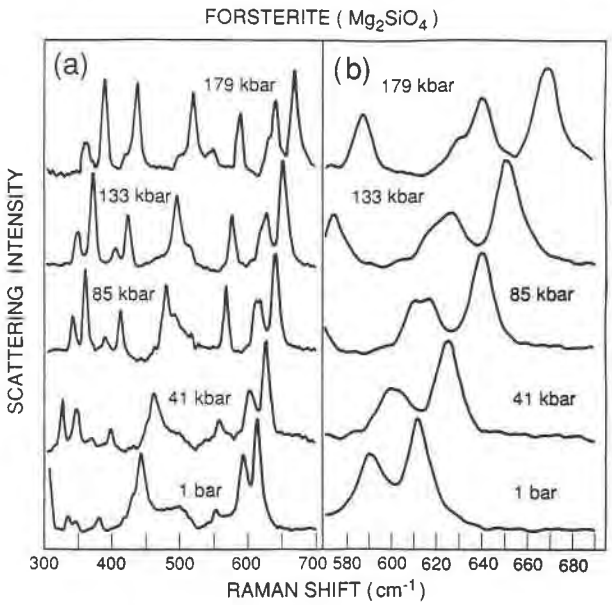

Fig. 4. Raman spectra of forsterite in the range 300–700 cm^{-1} at various pressures (**a**) and (**b**) Raman spectra of forsterite on an expanded scale showing the splitting of the 585-cm^{-1} Raman band at high pressures.

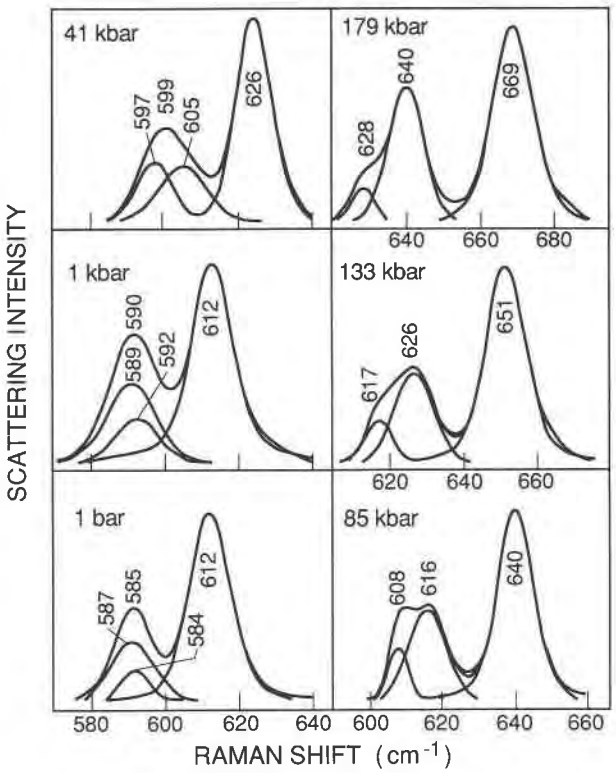

Fig. 5. The curve-fit determination of the positions and intensities of Raman spectra peaks 14 and 15 at various pressures for forsterite.

tively, at ~85, ~70, ~109, ~80, and ~90 kbar (Fig. 3a). Under quasi-hydrostatic pressure these bands show a break in their slopes, respectively, at ~90, ~70, ~80, ~106, and ~75 kbar (Fig. 3b). Table 2 lists the standard deviations of linear fits of Raman shift vs. pressure for these bands in the whole *P* range (0–179 kbar) and in the respective *P* range of 0–85 and 109–179 kbar. Standard deviations for fits to both the entire range (0–179 kbar) and to separate subranges have the same order, especially for peaks at 227 and 856 cm^{-1}, which have the same values. Based on this fact, it seems that the changes in slope are very small.

We found that the band at 585 cm^{-1} is indeed a doublet consisting of unresolved bands at 584 and 587 cm^{-1}. Both the bands in the doublet originate from the ν_4 internal mode of vibration but have different symmetries (e.g., Iishi, 1978; Chopelas, 1991). Because the pressure dependence of the bands within the doublet is different, the doublet seems to split at higher pressures (see Fig. 4a and 4b). We have repeated this experiment a number of times; the split is highly reproducible and reversible—the bands overlapped when the pressure decreased to 1 bar. We have determined the positions and intensities of these bands using the curve-fit method (Fig. 5). Their positions and pressure dependencies are (584 + 0.218) *P* and (587 + 0.280) *P* (cm^{-1}); in Table 1 these are marked as peak nos. 14 and 15, respectively. In the low-pressure range the relative intensity of peak no. 14 is greater than that of peak no. 15, whereas in the high pressure range the intensity of the latter is greater.

Chopelas (1990) reported that three bands at 183 (no. 1), 424 (no. 10), and 441 cm^{-1} (no. 12) of forsterite (Table 1) completely disappear above 91 kbar in the Raman spectrum. We observe at least two of these bands (10 and 12) clearly up to 179 kbar (see Fig. 6); however, their intensities are weaker. The 183-cm^{-1} band is also observed above 100 kbar but becomes weak with increasing pressure and difficult to measure because of interference

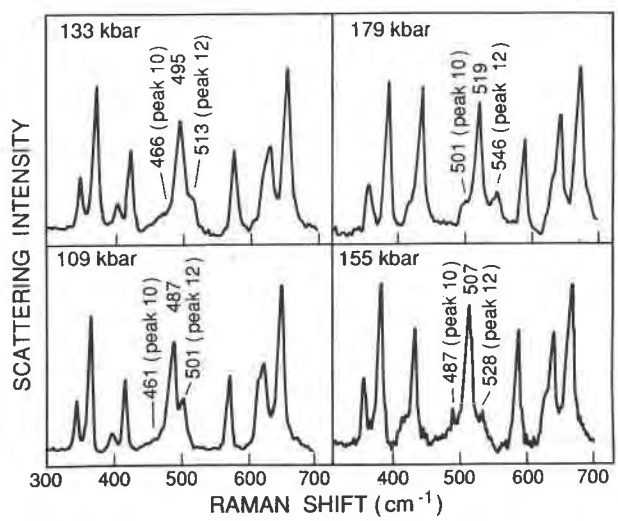

Fig. 6. Positions of Raman spectra showing bands at 424 cm^{-1} (10) and 441 cm^{-1} (12) at high pressures.

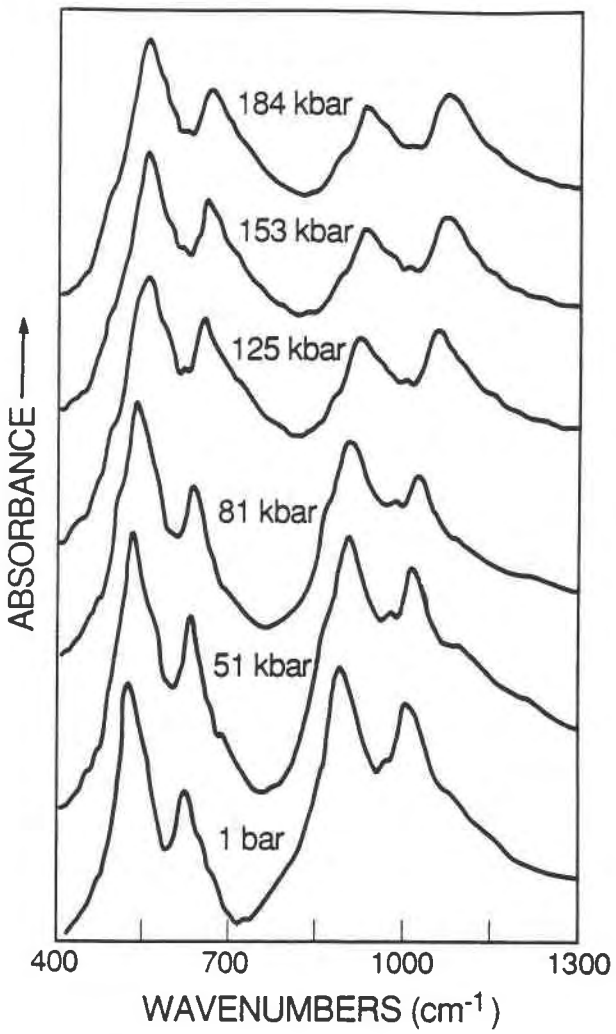

Fig. 7. Typical mid-IR spectra of forsterite from 1 atm to 184 kbar and at 20 °C.

from the strong Rayleigh tail and parasitic scattering. Our results show that no Raman bands become unobservable and no new bands appear on compression to 179 kbar.

Chopelas (1990) interpreted the loss of the bands and the change in the slope of six Raman bands as a second-order phase transition that is likely to be related to the olivine-spinel transition at high temperature. Single-crystal structure and compression studies have shown that forsterite transforms into the β-phase, exhibiting the structure of the so-called modified-spinel type under high pressure and temperature (Morimoto et al., 1969). According to Akimoto et al. (1976), the transformation occurs at a pressure of about 125 kbar and approximately 1000 °C. If a second-order transition indeed occurs, one would expect that under quasi-hydrostatic stress, the transition pressure would be lower (e.g., Bridgman, 1945; Adams and Sharma, 1981; Mammone et al., 1980b). One would also expect the parallel result of abruptly changing slope for the IR bands. Neither of these effects are observed in the present work, indicating that no second-order phase transition takes place at 91 kbar. The significant decrease in the intensities of the low-frequency bands and relative change in the intensities of the bands at 584 and 587 cm^{-1} above 80 kbar probably indicate change in the polarizability associated with these modes.

The effect of pressure on the crystal structure of forsterite was initially investigated with a single-crystal diffractometer up to 50 kbar at room temperature (Hazen, 1976; Hazen and Finger, 1980). According to these studies, the mean Si-O bond length was essentially unchanged up to 50 kbar, within experimental error. Kudoh and Takéuchi (1985) have studied the crystal structure of forsterite up to 149 kbar. According to them, the Si-O bonds in forsterite show a significant compression. The three A_{1g} modes of forsterite at 826, 856, and 966 cm^{-1} show continuous increase in frequency with increasing pressure (Table 1), indicating that there is some compression of the Si-O bonds. In addition, Kudoh and Takéuchi (1985) have shown that the Mg1-O distance ceases to decrease at about 80 kbar, whereas the Mg2-O bond shows a linear decrease with increasing pressure to 149 kbar. The change in the compression mechanism of forsterite above 80 kbar is most probably responsible for the observed break in the slope of the Raman bands and the change in the relative intensities of some of the Raman and infrared bands. The results of the present Raman investigation thus support the conclusions of Kudoh and Takéuchi (1985) that under high pressure the Si-O bonds in forsterite show significant compression and that there is change in the compression mechanism of forsterite above 80 kbar.

Infrared spectral data

Figure 7 shows a typical mid-IR spectrum of forsterite in the pressure range 1 bar to 184 kbar at 20 °C. The mid-IR bands of forsterite move to progressively higher frequencies and progressively broaden with pressure. Figure 8 shows the pressure dependencies for six mid-IR modes under quasi-hydrostatic conditions. The band positions have linear relations with pressure in this pressure range. We did not, however, observe a changing slope, $d\nu/dP$, and the disappearance of bands, as occurs in the Raman spectra. The pressure derivatives, mode Grüneisen parameters, and mode types are listed in Table 3. Because the IR bands of powdered samples are an average of several modes, mostly transverse optic (TO) and, secondarily, longitudinal optic (LO), the other parameters (i.e., γ_i) are also assumed to serve as average values. The differences in the pressure derivatives of the IR bands reported by different authors are large (see Table 3). Our values of pressure derivatives of IR bands of forsterite are higher than those reported by previous workers (Hofmeister et al., 1989; Xu et al., 1983). The difference may reflect the difficulties in measuring the frequencies of broad IR bands as well as inaccuracies in pressure measurements under quasi-hydrostatic conditions.

The mid-IR bands of forsterite have been assigned to Si-O stretching and bending modes (Hofmeister, 1987).

TABLE 3. Pressure derivatives, mode Grüneisen parameters, γ_i, and mode assignments for mid-IR vibrational modes of forsterite

Band no.	Present work			Hofmeister et al. (1989)			Xu et al. (1983)		Mode type, Hofmeister (1987)
	ν_{i0}	$d\nu_i/dP$	γ_i	ν_{i0}	$d\nu_i/dP$	γ_i	ν_{i0}	$d\nu_i/dP$	
1	516.5	0.202	0.50	482.8	0.145	0.38			ν_4
2	614.0	0.257	0.54	608.9	0.133	0.28	612.8	0.300	ν_4
3	845.5	0.258	0.39	835.7	0.305	0.47			ν_1
4	887.1	0.271	0.39	876.0	0.218	0.32	891.6	0.230	ν_3
5	962.3	0.238	0.32	924.9	0.169	0.23			ν_3
6	992.2	0.501	0.65	987.9	0.523	0.68	989.0	0.494	ν_3

The shift of the IR bands of forsterite is in response to compression of the unit cell and because of minor distortions of the SiO_4 group. The pressure derivatives of IR bands of forsterite are slightly lower than those of the corresponding Raman modes, a result implying relatively rigid behavior of the silica tetrahedron. This result is in agreement with X-ray studies (Merrill and Bassett, 1974; Kudoh and Takéuchi, 1985). It is evident from Table 1 that with the exception of Raman mode no. 2 (227 cm^{-1}), all the Raman bands associated with lattice modes (Mg2 translations, SiO_4 translations and rotations) have large values of the mode Grüneisen parameter, γ_i (>0.9); all Raman and IR bands (Tables 1 and 3) associated with the internal SiO_4 vibrations have small γ_i (<0.8). This result indicates that most of the compression of forsterite is caused by the compression of MgO_6 octahedra and that SiO_4 tetrahedra are relatively uncompressible.

Because of the overlapping of infrared bands, the low intensities of some peaks, and the presence of interference fringes, it is difficult to make accurate measurements of the width and area of IR bands. Nonetheless, the broadening of the IR bands is significant as pressure increases. This result suggests that IR absorption is more sensitive to crystal-field effects than is Raman scattering. The area under any given absorption peak (i.e., integrated intensity) is related to the number of atoms involved in the vibration. Hofmeister et al. (1989) have pointed out that, after the thinning effect of the gasket under pressure is accounted for, the peak area is expected to be independent of pressure, unless the sample undergoes a phase transition. Another possibility is that the deformation of the structure could cause a change in the permanent dipole moment associated with some of the modes and thus alter their intensities at high pressures.

A slight but definite increase in area for the IR band no. 2 (614 cm^{-1} assigned to ν_4) as pressure increases can be observed from Figure 7. In contrast, the area of IR band no. 4 (887 cm^{-1} assigned to ν_3) strongly and monotonically decreases as pressure increases. The mode no. 1 (516 cm^{-1}, assigned to ν_4) is always the strongest band in the pressure range used in the present study. The relative intensity ratios I_4/I_1 and I_6/I_1 decrease as pressure increases. These changes in the relative intensities of infrared bands may indicate change in the permanent dipole moment of SiO_4 groups because of deformation of crystal structure and SiO_4 tetrahedra. Hofmeister et al. (1989) have also observed change in the relative intensities of a number of far-IR and midinfrared bands of olivines.

SUMMARY AND CONCLUSIONS

We have investigated the effect of both hydrostatic and quasi-hydrostatic pressure on the Raman spectrum of forsterite to 200 kbar, and the effect of quasi-hydrostatic pressure on the mid-IR forsterite spectrum. Pressure dependencies of 21 Raman bands and six infrared bands of forsterite have been measured. Below 70 kbar under hydrostatic pressure, all the Raman bands show linear increase in their frequencies with increasing pressure. In the pressure range of 70–90 kbar, five of the Raman bands show a slight break in their slopes, which is attributed to change in the compression mechanism in forsterite at high pressures.

A comparison of the Raman data of forsterite under hydrostatic and quasi-hydrostatic pressures shows that the Raman spectrum is not very sensitive to quasi-hydrostatic stress. The small differences in the $d\nu/dP$ values of Raman bands under hydrostatic and quasi-hydrostatic

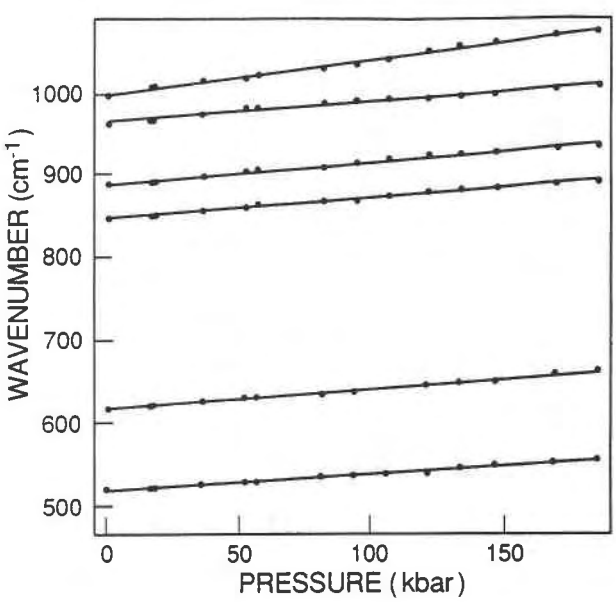

Fig. 8. The pressure dependence for six mid-IR modes under quasi-hydrostatic pressure with KBr as pressure transmitting medium.

pressures can account for some of the different values of the slope of Raman bands reported in the literature.

In the mid-infrared spectra, the six internal modes of SiO_4 units of forsterite change linearly with pressure to 184 kbar, in agreement with the results of previous workers. With increasing pressure, the relative integrated intensity of the 614-cm^{-1} IR band (one of the bending modes of SiO_4) is found to increase with increasing pressure, whereas that of the 887-cm^{-1} IR band (one of the Si-O stretching modes of SiO_4) strongly decreases above 81 kbar. The observed decrease in the intensities of IR bands at high pressures is attributed to distortion of SiO_4 tetrahedra.

Acknowledgments

We would like to thank John B. Bates of Oak Ridge National Laboratory for providing the forsterite crystal. This work was supported in part by NSF grant EAR-8915830. S.K.S. would like to thank the Earth Science Equipment program of NSF for providing partial financial support for the micro-Raman spectroscopic facility. The authors would like to thank G. Fiquet and an anonymous referee for their constructive suggestions on an earlier version of this manuscript. This is School of Ocean and Earth Science and Technology contribution no. 3141.

References cited

Adams, D.M., and Sharma, S.K. (1981) Vibrational spectroscopy at high pressures. Part 30. Raman study of silver, ammonium and potassium nitrites. Journal of the Chemical Society, Faraday Transaction II, 77, 1263–1272.

Akimoto, S., Matsui, Y., and Syono, Y. (1976) High pressure chemistry of orthosilicate and the formation of mantle transition zone. In R.G. Strens, Ed., Physics and chemistry of minerals and rocks, p. 327–363. Wiley, London.

Besson, J.M., Pinceaux, J.P., and Anastopoulos, C. (1982) Raman spectra of olivine up to 65 kbar. Journal of Geophysical Research, 87, 10773–10775.

Bridgman, P.W. (1945) The compression of twenty-one halogen compounds and eleven other simple substances to 100,000 kg/cm^2. Proceedings of the American Academy of Arts and Sciences, 76, 1–7.

Brown, G.E. (1980) Olivines and silicate spinels. In Mineralogical Society of America Reviews in Mineralogy, 5, 275–381.

Chopelas, A. (1990) Thermal properties of forsterite at mantle pressure derived from vibrational spectroscopy. Physics and Chemistry of Minerals, 17, 149–156.

——— (1991) Single crystal Raman spectra of forsterite, fayalite and monticellite. American Mineralogist, 76, 1101–1109.

Gillet, P., Richet, P., Guyot, F., and Fiquet, G. (1991) High-temperature thermodynamic properties of forsterite. Journal of Geophysical Research, 96, 11805–11816.

Graham, E.K., Jr., and Barsch, G.R. (1969) Elastic constants of single-crystal forsterite as a function of temperature and pressure. Journal of Geophysical Research, 74, 5949–5960.

Guyot, F., and Reynard, B. (1992) Pressure-induced structural modifications and amorphization in olivine compounds. Chemical Geology, 96, 411–420.

Hazen, R.M. (1976) Effect of temperature and pressure on the crystal structure of olivine. American Mineralogist, 64, 1280–1293.

Hazen, R.M., and Finger, L.W. (1980) Crystal structure of forsterite at 40 kbar. Carnegie Institution of Washington Year Book, 79, 364–367.

Hofmeister, A.M. (1987) Single-crystal absorption and reflection infrared spectroscopy of forsterite and fayalite. Physics and Chemistry of Minerals, 14, 499–513.

Hofmeister, A.M., Xu, J., Mao, H.K., Bell, P.M., and Hoering, T.C. (1989) Thermodynamics of Fe-Mg olivines at mantle pressure: Mid- and far-infrared spectroscopy at high pressure. American Mineralogist, 74, 281–306.

Iishi, K. (1978) Lattice dynamics of forsterite. American Mineralogist, 63, 1198–1208.

Jayaraman, A. (1983) Diamond anvil cell and high-pressure physical investigations. Reviews of Modern Physics, 55, 65–108.

Kudoh, Y., and Takéuchi, Y. (1985) The crystal structure of forsterite Mg_2SiO_4 under high pressure up to 149 kb. Zeitschrift für Kristallographie, 171, 291–302.

Kumazawa, M., and Anderson, O.L. (1969) Elastic moduli, pressure derivatives and temperature derivatives of single-crystal olivine and single-crystal forsterite. Journal of Geophysical Research, 74, 5961–5972.

Lam, P.K., Yu, R., Lee, M.W., and Sharma, S.K. (1990) Structure distortion and vibrational modes in Mg_2SiO_4. American Mineralogist, 75, 109–119.

Mammone, J.F., Sharma, S.K., and Nicol, M. (1980a) Raman spectra of methanol and ethanol at pressures up to 100 kbar. The Journal of Physical Chemistry, 84, 3130–3134.

——— (1980b) Raman study of rutile (TiO_2) at high pressure. Solid State Communications, 34, 799–802.

Mao, H.K., and Bell, P.M. (1978) Design and varieties of the megabar cell. Carnegie Institution of Washington Year Book, 77, 904–908.

Mao, H.K., Bell, P.M., Shaner, J., and Steinberg, D. (1978) Specific volume measurement of Cu, Mo, Pd, and Ag and calibration of the ruby R_1 fluorescence pressure gauge from 0.06 to 1 Mbar. Journal of Applied Physics, 49, 3276–3283.

Merrill, L., and Bassett, A. (1974) Miniature diamond anvil pressure cell for single crystal x-ray diffraction studies. Review of Scientific Instruments, 45, 290–294.

Morimoto, N., Akimoto, S., Koto, K., and Tokonami, M. (1969) Modified spinel, beta-manganous orthogermanate: Stability and crystal structure. Science, 165, 586–588.

Petricevic, V., Gayen, S.K., and Alfano, R.R. (1988) Laser action in chromium-activated forsterite for near-infrared excitation: Is Cr^{4+} the lasing ion? Applied Physics Letters, 53, 2590–2592.

Reynard, B. (1992) Single-crystal infrared reflectivity of pure Mg_2SiO_4 forsterite and $(Mg_{0.86}Fe_{0.14})_2SiO_4$ olivine. Physics and Chemistry of Minerals, 18, 19–25.

Sharma, S.K. (1990) Applications of Raman spectroscopy in earth and planetary sciences. In K. Gopalan, V.K. Gaur, B.L.K. Somayajulu, and J.D. McDougall, Eds., From mantle to meteorites: A Festschrift for Devendarlal, p. 263–308. Indian Academy of Science, Bangalore, India.

Sharma, S.K., and Urmos, J.P. (1987) Micro-Raman spectroscopic studies of materials at ambient and high pressures with CW and pulsed lasers. In R.H. Geiss, Ed., Microbeam analysis—1987, p. 133–136. San Francisco Press, San Francisco.

Sharma, S.K., Cooney, T.F., and Wang, S.Y. (1992) Effect of high P and T on olivines: A Raman spectral study. In R.K. Singh, Ed., Recent trends in high pressure research, Proceedings of XIII AIRAPT International Conference of High Pressure Science and Technology, p. 614–619. Oxford and IBH Publishing, New Delhi, India.

Sugimoto, A., Segawa, Y., Yamaguchi, Y., Nobe, Y., Yamagishi, K., Kim, P.H., and Namba, S. (1989) Flash lamp tuned pumped tunable forsterite laser. Japanese Journal of Applied Physics, 28, L1833–L1835.

Webb, S.L. (1985) Elasticity of some mantle minerals. Ph.D. dissertation, Australian National University, Canberra.

Xu, J., Mao, H.K., Weng, K., and Bell, P.M. (1983) High pressure Fourier-transform infrared spectra of forsterite and fayalite. Carnegie Institution of Washington Year Book, 82, 350–352.

Manuscript received May 5, 1992
Manuscript accepted January 26, 1993